Journal of Cleaner Production 234 (2019) 200–207

Contents lists available at ScienceDirect

Journal of Cleaner Production

journal homepage: www.elsevier.com/locate/jclepro

A novel technique in the preparation of environmentally friendly cellulose nanofiber/silk fibroin fiber composite films with improved thermal and mechanical properties

Chieko Narita, Yoko Okahisa, Kazushi Yamada*

Faculty of Fiber Science and Engineering, Kyoto Institute of Technology, Matsugasaki, Sakyo-ku, Kyoto, 606-8585, Japan

ARTICLE INFO

Article history:
Received 7 January 2019
Received in revised form
27 May 2019
Accepted 19 June 2019
Available online 21 June 2019

Handling editor: Jun Bi.

Keywords:
Silk fibroin
Nanofiber
Composite film
Grinder

ABSTRACT

In this paper, we report a novel technique which enabled us to easily and directly obtain a silk fibroin (SF) solution without the use of organic solvents by applying a simple grinder for silk cocoons. In addition, we successfully prepared cellulose nanofiber/silk fibroin (CNF/SF) nanofiber composite films using a filtration and pressing method from a slurry solution blended with a CNF solution. The peak temperature of the thermal decomposition of the SF nanofibers prepared using the new method developed in this research was improved by more than 13 °C, and that of the composite films compounded with more than CNF 50 wt% showed almost the same temperature as the CNF film. In addition, the mechanical properties of the CNF/SF nanofiber composite films were increased with increasing the amount of CNF. These results strongly suggest that the SF solution prepared using our novel method has advantages of superior thermal and mechanical properties compared with that prepared by a conventional method using a concentrated neutral salt solution. Additionally, this result indicates the film manufacturing method having advantages of water pollution reduction and energy saving.

© 2019 Elsevier Ltd. All rights reserved.

1. Introduction

Fibroin is a type of fibrous protein, occupying 70% of the cocoon yarns of insects and spiders, and is a major component in the silk thread of silkworms. In particular, silk fibroin (SF) obtained from domesticated silkworms has been considered in numerous studies, focusing on its detailed molecular structure and higher-order structural changes, its use in artificial skin and culture substrates, its biocompatibility, and its application in supplements, among other areas (Bhardwaj and Kundu, 2011; Chen et al., 2014; Jin et al., 2013; Lee et al., 2018; Mehrabani et al., 2018; Zhou et al., 2017). SF forms a strong hydrogen bond between molecular chains, takes an antiparallel β-sheet type crystal structure, and is insoluble in water (Lu et al., 2010). Therefore, to produce films and nanofibers, it is necessary to prepare an aqueous solution by dissolving the SF in an organic solution and then dialyzing it. In a traditional dissolution method of silk fibroin, the material is dissolved in a concentrated neutral salt solution; the solution is then placed in a cellulose tube and dialyzed with pure water for about 1 week to remove any existing ions (Du et al., 2009; Yamada et al., 2003; Zhu et al., 2012). The higher-order structure of SF in an aqueous solution obtained through this method is of a random coil type (Yamada et al., 2003). However, this sample preparation procedure is very complicated and lengthy, and furthermore it necessitates the use of an organic solvent. From the viewpoint of environmental compatibility and economic efficiency, preparation of bio-based materials in a short time without using organic solvents is strongly desired.

On the other hand, many attempts have been made to improve the mechanical properties or create new functions by blending SF with other polymers, such as cellulose (Cho et al., 2014; Kim et al., 2017; Marsano et al., 2008; Yang et al., 2000), hydroxyapatite (Farokhi et al., 2018; Ming et al., 2014), sodium carboxymethyl cellulose (Kundu et al., 2011; Singh et al., 2016), or other materials employed for a variety of tissue engineering applications. According to previous studies (Feng et al., 2017; Kim et al., 2017; Noishiki et al., 2002; Yang et al., 2000), cellulose nanofibers and cellulose microcrystals act as a reinforcing material for fibroin films; however, in these researches, fibroin was dissolved in concentrated neutral salts such as lithium bromide for the preparation of a fibroin solution. The use of organic solvents is uneconomical and environmentally unfriendly from the viewpoint of water shortage

* Corresponding author.
E-mail addresses: narita@kit.ac.jp (C. Narita), okahisa@kit.ac.jp (Y. Okahisa), kazushi@kit.ac.jp (K. Yamada).

https://doi.org/10.1016/j.jclepro.2019.06.215
0959-6526/© 2019 Elsevier Ltd. All rights reserved.

crisis and water pollution (Gleick, 2003; Xie et al., 2018). Therefore, a novel preparation method without using organic solvent for SF solutions and SF films needs to be explored.

Grinder treatment has been widely used in the fibrillation of woody biomass with the attraction of high efficiency and low pollution. Therefore, it is hypothesized that grinder treatment could be a feasible method to fibrillate SF. If it becomes possible to easily prepare a solution of SF using a grinder, similar to the method used to prepare CNF without the usage of an organic solvent, CNF/SF composite films fabricated using these solutions could have numerous potential applications. This study focuses on the physical property evaluation of CNF/SF nanofiber composite film made from the fibroin solution and cellulose nanofiber solution prepared using a grinder. The changes in the surface morphology, structure, thermal properties, and mechanical properties of CNF/SF nanofiber composite films are discussed for different CNF contents (0%, 20%, 50%, 80%, and 100%), based on the results of SEM, FT-IR, Raman spectroscopy, TGA, and tensile test analyses.

2. Materials and methods

2.1. Materials

A simple method for directly preparing an SF nanofiber solution without dissolving in a concentrated neutral salt solution is as follows. First, raw silk was ground and degummed with a 0.9 wt% Na_2CO_3 solution at 95 °C for 120 min to remove the sericin. The samples were then rinsed with distilled water, and an aqueous solution of purified silk fibroin was obtained. The water slurry with a 1 wt% undried purified silk fibroin sample was passed four times through a grinder (MKCA6-3, Masuko Sangyo Co. Ltd., Japan) at 1500 rpm with the grinding stones (NKGC6-120, Masuko Sangyo Co. Ltd., Japan) pressed closely together.

Cellulose nanofibers (CNFs) were supplied from Daio Paper Co., Japan. The CNFs were bleached chemical pulp made from hardwood chips, and were applied in a slurry-like aqueous solution with a concentration of 2 wt%. Images of CNF and SF slurry are shown in Fig. 1.

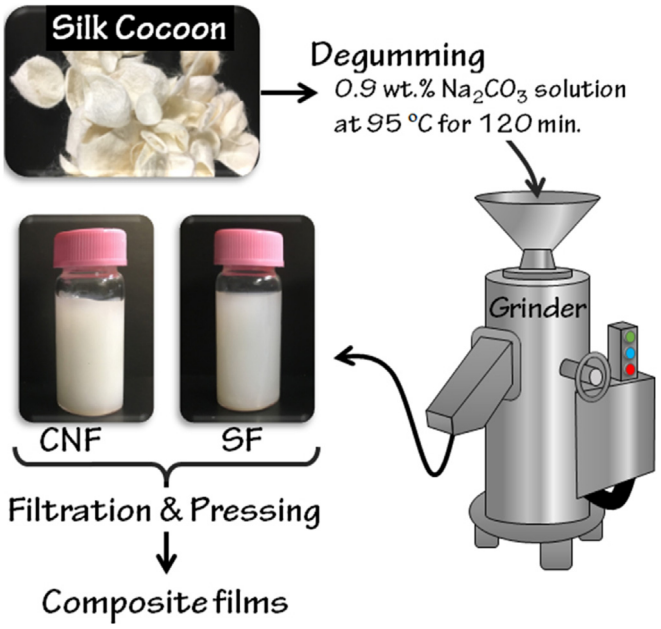

Fig. 1. Schematic illustration of processing of composite films using a simple method.

2.2. Preparation of CNF/SF nanofiber composite films

The slurry of CNF and SF was blended to prepare the sample films. The composite films with a diameter of 90 mm were obtained from 70 g of fibrillated slurry with a fiber content of 1 wt% through filtration, pressing, and drying at 40 °C under a vacuum. The component ratio of the composite films produced is shown in Table 1. The thickness of the film was adjusted to approximately 50–100 μm. A schematic illustration of the composite film preparation process is shown in Fig. 1.

2.3. Characterization of CNF/SF nanofiber composite films

2.3.1. Scanning electron microscope (SEM) observation

A scanning electron microscope (SEM, JSM-6010LA, JEOL Co. Ltd., Japan) was used to observe the surface morphology of the CNF/SF fiber composite films and fractured surface morphology after the tensile test. The electron accelerating voltage was set at 10 kV. All specimens were coated in gold using an ion-sputtering machine (JFC-1600 Auto Fine Coater, JEOL Co. Ltd., Japan) before the SEM observations. Additionally, an energy dispersive X-ray spectrometry (EDS) analysis was conducted to obtain quantitative information of the composition ratio for the CNF/SF fiber composite films.

2.3.2. Fourier-transform infrared (FT-IR) spectroscopy

The CNF/SF fiber composite films were analyzed using attenuated total reflection (ATR) mode of FT-IR spectroscopy (GX, 2000 FT-IR spectrometer, PerkinElmer, Inc., USA) to measure the changes in functional groups induced through a purification of cellulose, and to compare them among the samples. Spectra were collected within the range of 4000–800 cm^{-1} at a resolution of 4 cm^{-1}, and the number of scans was set at 16 for each sample.

2.3.3. Raman spectroscopy

The samples used for the Raman spectroscopic analysis were excited using a linearly polarized 633 nm laser (LabRAM HR-800, HORIBA Co., Ltd., Japan), and the excitation beam was directed toward the sample compartment of a properly modulated confocal microscope (BX-41, Olympus Corp., Japan). The exposure time was set at 2.0 s, and the number of scans was set at ten for single spectrum measurements. In contrast, using SWIFT mode, the 2D imaging measurements were conducted using a 100 μm × 100 μm square with a measurement point spacing of 2 μm. The total number of measurement points per image was 2601. The exposure time was set to 2.0 s/point and the number of scans was set to one per point.

2.3.4. Thermogravimetric analysis (TGA)

The thermostability of the CNF/SF fiber composite films was characterized using a thermogravimetric analyzer (TGA) (Discovery TGA, TA Instruments, USA), conducted at a rate of 20 °C/min from 50 °C to 800 °C. The measurements were applied in a nitrogen atmosphere at a flow rate of 50 ml/min.

Table 1
Component ratio of the CNF/SF composite films produced.

	CNF/wt.%	SF/wt.%
SF100	0	100
SF80	20	80
SF50	50	50
SF20	80	20
CNF	100	0

2.3.5. Tensile test

The mechanical properties of the CNF/SF fiber composite films were characterized using tensile testing. A dumbbell-shaped specimen (ISO 527–2:2012, Model 5B) was cut out of each sample film using a Super Dumbbell cutter (SDL-100: Dumbbell Co. Ltd., Japan). The tensile tests were conducted using a Table Top Universal Testing Machine (MCT-2150, A&D Co. Ltd, Japan) at 25 °C at a crosshead speed of 50 mm/min. The average values ± standard deviations of the tensile modulus, tensile strength, and strain at break were evaluated using five independent specimens.

3. Results and discussion

3.1. Surface morphology and higher-order structures of composite films

Fig. 2 shows optical photographs of CNF/SF nanofiber composite films. As shown in the image, the CNF film surface looks uniform and highly transparent, while the film surface has whiteness and roughness with increasing the content of SF. Therefore, SEM observation was performed to further evaluate these surface structures in detail. Fig. 3 shows an SEM photograph of an SF film that was successfully obtained for the first time from SF nanofibers defibrated and refined using a grinder without dissolving in a concentrated neutral salt. Fibers with a width of approximately 10 μm observed on the surface of the composite film were increased when increasing the amount of SF blended for the CNF. The diameter of each SF thread is about 10 μm (Zhang et al., 2002), which coincides with the larger fiber diameter observed on the composite film surface. Therefore, it is considered that the SF threads are partially contained in the slurry solution of silk fibroin obtained through direct fibrillation with a grinder, whereas most of the components in the solution consist of SF nanofibers owing to the slurry formation. However, this suggests that thick fibers are not present on the CNF film surface, as shown on the SF film, and are completely nanofiberized. The results of the EDS analysis of the surface of these CNF/SF nanofiber composite films are plotted in Fig. 4. Cellulose fibers are composed of glucose, and nitrogen atoms are not contained in the molecular chain. In contrast, SF is a protein composed of essential amino acids having nitrogen atoms such as glycine or alanine. Therefore, among the C, N and O data obtained through the EDS analysis, data on the nitrogen atoms were selected herein. As shown in this graph, the ratio of nitrogen atoms increased with an increase in the amount of SF. To obtain detailed chemical structure information, FT-IR measurements were carried out on these composite films.

Fig. 5 shows the FT-IR spectra of the CNF/SF nanofiber composite films. In the spectra from SF100, SF80, and SF50, absorption bands of amides I (C=O stretching) of approximately 1625 cm^{-1}, amide II (N–H deformation and CN stretching) of approximately 1518 cm^{-1}, and amide III (CN stretching and N–H deformation) of approximately 1265 cm^{-1} were observed. These peaks reflect the silk II structure of *Bombyx mori* silk fibroin (Tsuboi et al., 2001; Yamada et al., 2003), i.e., a secondary structure with an antiparallel β-sheet structure. It is known that the secondary structure of silk threads ejected by silkworms is an antiparallel β-sheet structure (Motta et al., 2002). Therefore, this indicates that the secondary structure of the fibrillated SF nanofibers from a cocoon when using a grinder retains the original conformation without any changes. However, characteristic peaks of cellulose were observed in the spectra of CNF, SF20, SF50, and SF80 (Okahisa et al., 2018). The absorption at 3345 cm^{-1} relates to the stretching of the O–H groups, and that at 2911 cm^{-1} relates to the C–H stretching. Two absorption bands at 1161 and 897 cm^{-1} arise from the C–O–C stretching at the β-(1–4)-glycosidic linkages. Strong peaks at 1056 and 1034 cm^{-1} are attributed to the C–O stretching (Liu et al., 2006). Thus, we showed the change in higher-order structure owing to the difference in the composition ratio of CNF/SF nanofiber composite films using FT-IR spectroscopy. However, it is difficult to know the molecular structure, such as the entanglement and orientation of the molecular chains, in the composite film owing to the larger spot diameter of the FT-IR. Therefore, microscopic Raman mapping measurements were carried out to measure the detailed structure of the CNF and SF molecules in these composite films.

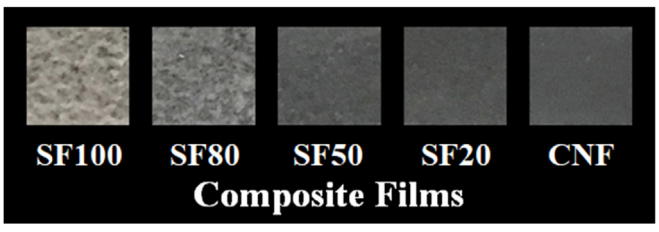

Fig. 2. Photo images of CNF/SF nanofiber composite films for each content.

There have been few studies conducted on CNF and fibroin using microscopic Raman spectroscopy. However, because a laser beam can be focused using an objective lens, the spot diameter of the measurement is extremely small at about 1 μm. Therefore, Raman spectroscopy has a high resolution, and is a powerful technique for obtaining information on the molecular structure of polymers. Fig. 6 shows the Raman spectra of these composite films. A typical Raman spectrum obtained from an SF film shows some characteristic peaks, where the Raman band at 1665 cm^{-1} corresponds to amide I (Monti et al., 1998), and the Raman bands at 1227 and 1262 cm^{-1} correspond to amide III (Monti et al., 1998). Additionally, the Raman band at 1087 cm^{-1} corresponds to the C–C stretching vibration. These four characteristic peaks are attributed to the antiparallel β-sheet structure of SF (Monti et al., 1998). In contrast, a typical Raman spectrum obtained from a CNF film shows certain characteristic peaks, where the Raman bands at 1095 and 1117 cm^{-1} correspond to the carbonyl (C–O) stretching mode (Wiley and Atalla, 1987), and the band at 2890 cm^{-1} corresponds to CH and CH_2 stretching modes (Wiley and Atalla, 1987). As shown in the FT-IR measurement results in Fig. 5, it was found that the spectrum of the CNF changes to the spectrum of fibroin as the amount of blended fibroin increases.

Fig. 7 (a) shows 2D chemical mapping images of the CNF/SF nanofiber composite films, SF20, SF50, and SF80. A red color corresponds to CNF-rich parts, and a green color corresponds to SF-rich parts. The green color area is increased with an increase in the amount of SF. Note that very small amounts of CNF and SF nanofibers are not shown as mapped colors, and the color of the dominant component at each measurement point is displayed on the mapped image. Therefore, this schematic illustration is completely divided into two colors, red and green, as rich domains, respectively. In particular, the width of the green thick thread-like structure is about 10 μm, which is consistent with the diameter of the original SF fibers. Therefore, the SF fibers were successfully observed using microscopic Raman spectroscopy. In contrast, the red area corresponding to the CNF rich parts seems to be adsorbed or entangled around the SF threads. These schematic illustrations are depicted in Fig. 7 (b). We consider the entanglement structure of the molecular chains of the CNF and SF in the composite films to be clearly observable through the use of microscopic Raman spectroscopy. From these results, we successfully fabricated CNF/SF nanofiber composite films from an SF slurry solution prepared without the use of a concentrated neutral salt solution.

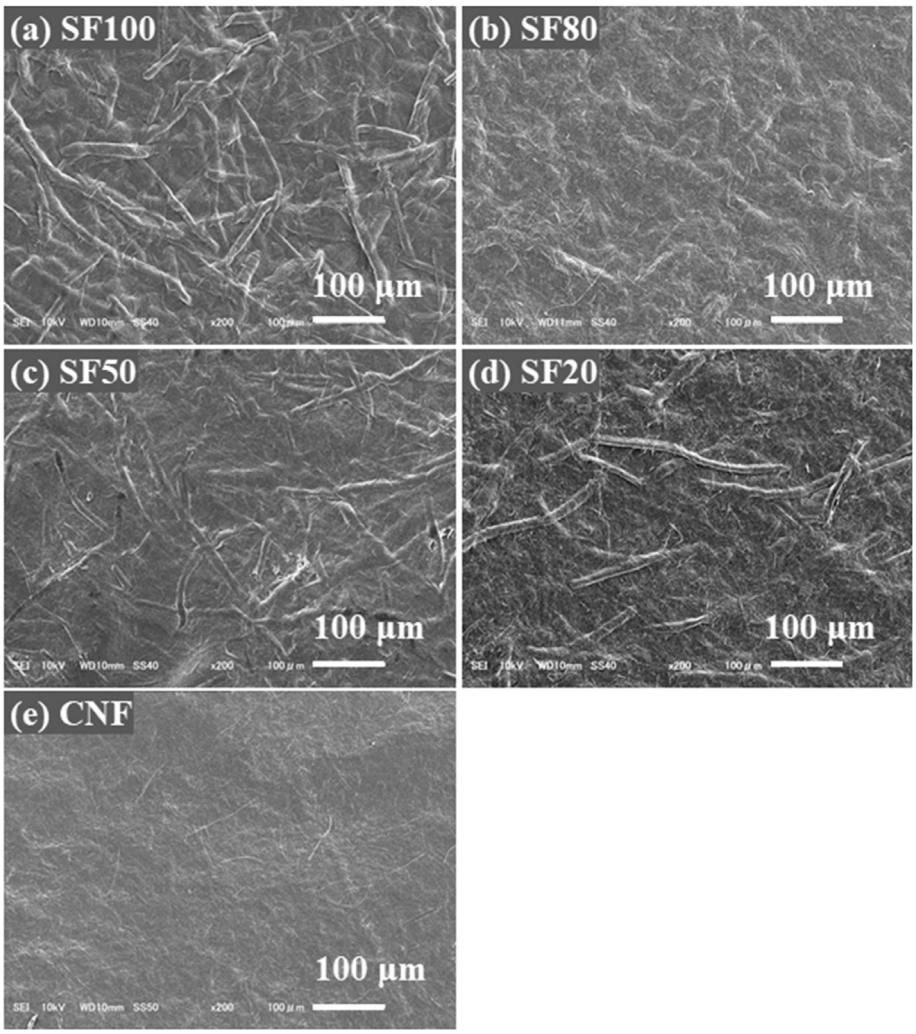

Fig. 3. (a)–(e) SEM images of each composite film surface.

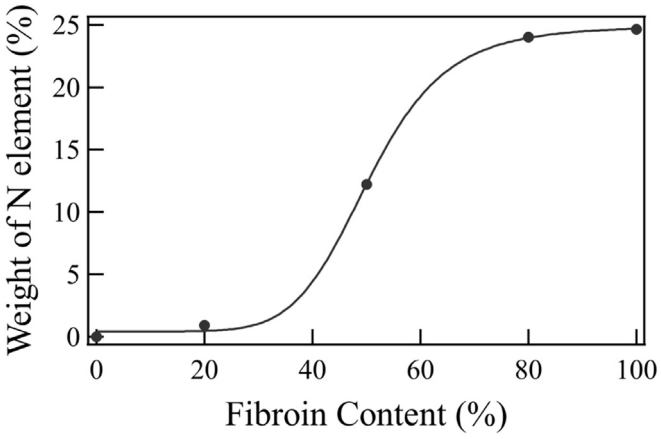

Fig. 4. Weight of N electron (%) plot for each content film by EDS analysis.

3.2. Thermal properties of composite films

TGA measurements were conducted for evaluating the thermal resistance of the CNF/SF nanofiber composite films. Fig. 8 shows the results of the TGA traces and derivation weight curves of these samples with a temperature range of 50–800 °C. The onset temperature of weight loss from thermal decomposition is ~300 °C in any composite film, although the weight of the final residue decreases as the amount of blended CNF increases. Fig. 8 (b) shows the derivation curves of each TGA chart used to evaluate the weight loss rate. From this graph, it can be seen that differential peaks occur at approximately 313 °C and 355 °C, which are considered to correspond to the peaks of the SF and CNF nanofibers, respectively. In general, the weight loss peak of SF dissolved in a concentrated neutral salt occurs at approximately 270–300 °C (Lawrence et al., 2010; Yuan et al., 2010), and the thermal decomposition temperature of the SF nanofibers prepared using the new method developed in this study was improved by more than 13 °C. The improvement in thermal stability is attributed to the higher order structure of silk fibroin (Gil et al., 2006; Okahisa et al., 2019). That is, the β-sheet structure leads to higher thermal stability. In addition, no peaks in the derivation weight at approximately 313 °C were found in the compounding amount of SF (50%), and it was found that thermal decomposition occurred at approximately 355 °C owing to the presence of CNF. This result indicates that adding about half of the cellulose nanofibers can greatly improve the thermal resistance properties of silk fibroin. It is considered that as the fiber surface of the compounding amount of more than CNF 50 wt% is covered with CNF from results of Raman images, the

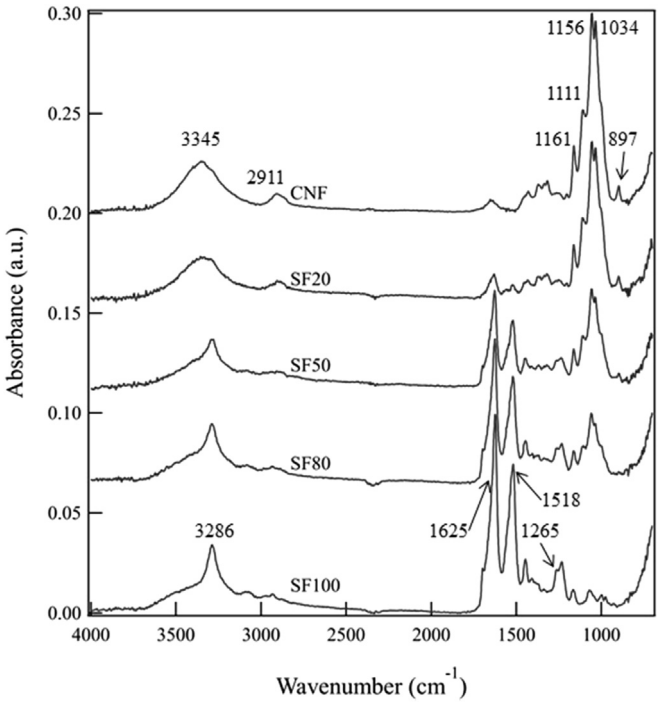

Fig. 5. FT-IR spectra of each composite film.

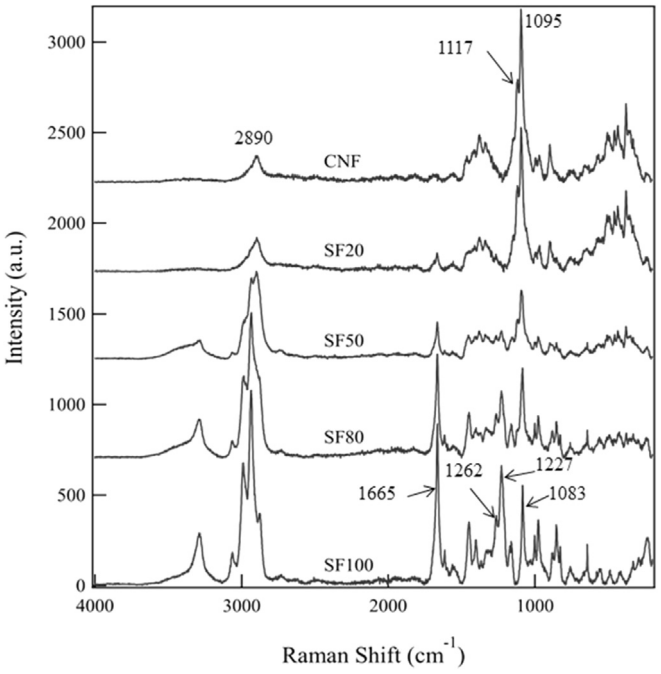

Fig. 6. Raman spectra of each composite film.

thermal decomposition property was improved because of inhibiting heat transfer to SF fibers.

3.3. Mechanical properties of composite films

To evaluate the mechanical properties of the prepared composite films, a tensile test was conducted using a dumbbell-shaped specimen. Table 2 lists the tensile properties, and Fig. 9 shows the stress–strain curves and fractured surface, of the composite films after the tensile test was applied. As can be seen from the table and graph, the tensile modulus and tensile strength were increased with an increase in the amount of CNF. The strain at break also was increased with the amount of CNF, similar to the tensile strength, whereas the strain at break in SF50 showed the longest value. From this result, it is thought that CNF plays an important role in improving the mechanical properties of an SF film. In addition, the mechanical characteristics of the CNF/SF composite films in this study were found to be superior to those of a past study (Noishiki et al., 2002). According to the previous research (Yano and Nakahara, 2004), the increase in microfibrils can form more hydrogen bonds between cellulose fibers, and the web-like network in nanometer units causes high interactive forces between CNFs. As a result, it is believed that the mechanical properties of the prepared sheet film are increased. Also, in this study, since silk fibroin is a hydrophilic fibrous protein and has many hydroxyl groups as functional groups, so the interaction between silk fibroin and cellulose nanofibers becomes large, and both fibers are easily entangled. This leads to the cellulose nanofibers reinforcing the silk fibroin film. As shown in Fig. 10, the morphology was lumpy on the fractured surface of SF100, and a few SF fibers with a diameter of 10 μm were observed there. SF fibers were not observed on the fractured surface of SF80, although the unevenness of the fractured surface was large, similar to that of SF100. In addition, it was found that both the left and right sides of the fractured surface in the SEM image, that is, the vicinity of the film surface, formed a layered structure, such as a Mille-feuille structure. In contrast, the fractured surfaces of SF50, SF20, and CNF showed a similar fractured surface shape, and it turned out that all surfaces, from the surface layer to the center layer, formed a Mille-feuille structure and had a dense cross-sectional formation. This indicates that CNF is packed between the SF fibers and molecular chains, and plays an important role as a reinforcing material for the SF film. These results are supported by the microscopic images from the Raman mapping analysis, as shown in Fig. 7. That is, as a result of CNF playing the role of the skin layer of SF fibers, it is considered that the tensile strength of SF 50 and SF 20 showed the similar values as CNF. Differences in these layered structures influence the tensile properties, resulting in an improvement in the elastic modulus, tensile strength, and strain at break.

3.4. Energy efficiency analysis

Energy efficiency of a novel technique using the grinder for SF was evaluated by dialyzing efficiency and specific energy consumption, a comparison was carried out with the conventional dissolution method. In a conventional dissolution method of SF, the material is dissolved in a concentrated neutral salt (LiBr) solution for 4 h at 60 °C; the solution is then placed in a cellulose tube and dialyzed with tap water for about 1 week to remove any existing ions as shown in Fig. S1 (Supplementary Materials). According to the calculation results (Tables S1, S2, and S3 of supplementary materials), the fibroin solution preparation time, power consumption, and cost by the grinder method can be reduced to 0.19%, 62.5%, and 0.28%, respectively, as compared with the conventional method. Further, as seen from Fig. S1 and Table S2, the grinder method does not use a reagent such as lithium bromide, so there is no influence of water pollution. Thus, this grinder treatment method has very lower processing cost and time than that of the conventional method of preparing the SF solution. This process has technical, commercial and ecological feasibility. Combined with the degumming method of raw silk via steam treatment (Wang et al., 2018), it will be a completely clean and economical film fabrication method.

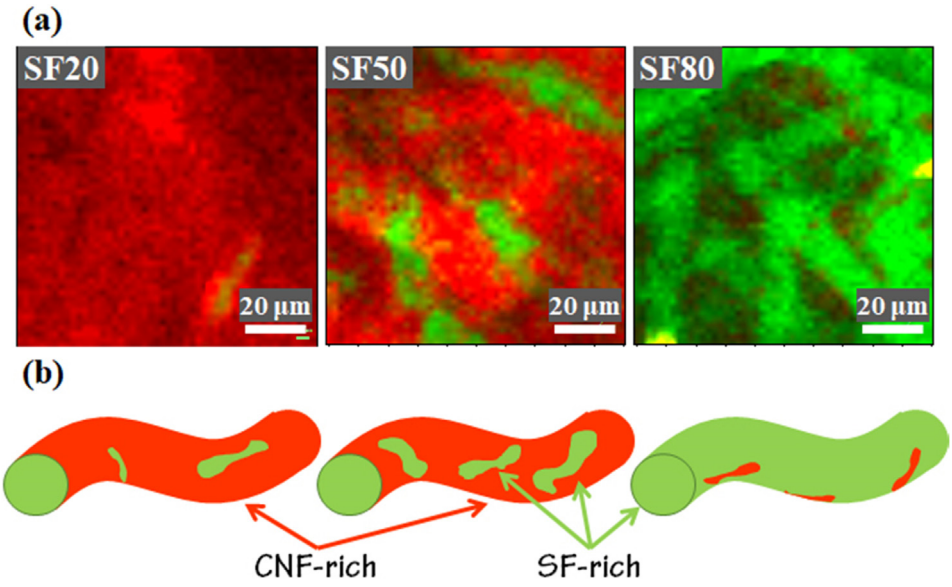

Fig. 7. (a) Surface 2D mapping for SF20, SF50, and SF80, and (b) schematic illustration of SF and CNF shown in mapping results.

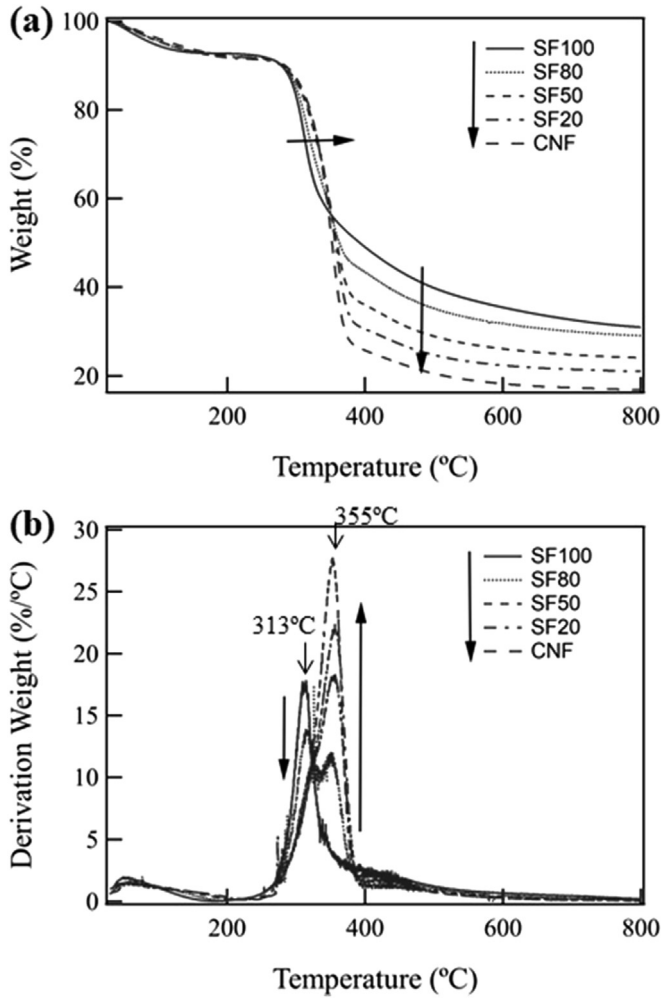

Fig. 8. TGA results of each composite film: (a) weight (%) curves and (b) derivation weight (%/°C) curves.

Table 2
Tensile properties of CNF/SF composite films.

	Tensile modulus/GPa	Tensile strength/MPa	Strain at break/-
SF100	3.01	42.8	0.023
SF80	7.20	134.0	0.027
SF50	9.19	230.2	0.110
SF20	9.35	248.7	0.080
CNF	10.59	296.3	0.105

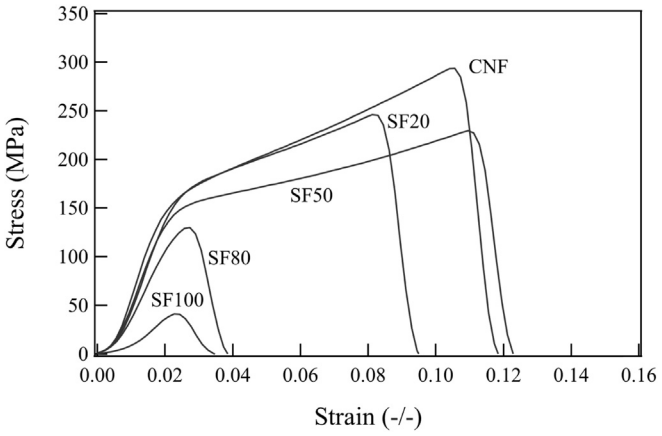

Fig. 9. Stress-Strain curves of each composite film after tensile test.

4. Conclusions

This research aimed to provide a novel technique based on material technology enabling the fabrication of bio-based nanofiber composite films consisting of cellulose and silk fibroin nanofibers. Herein, we demonstrated a simple technique using a grinder for silk cocoons to obtain a slurry solution without the use of organic solvents such as a concentrated neutral salt solution. We successfully prepared CNF/SF nanofiber composite films with high mechanical properties using a filtration and pressing method from a slurry solution blended with a CNF solution. As the results show, the thermal decomposition temperature of the SF nanofibers

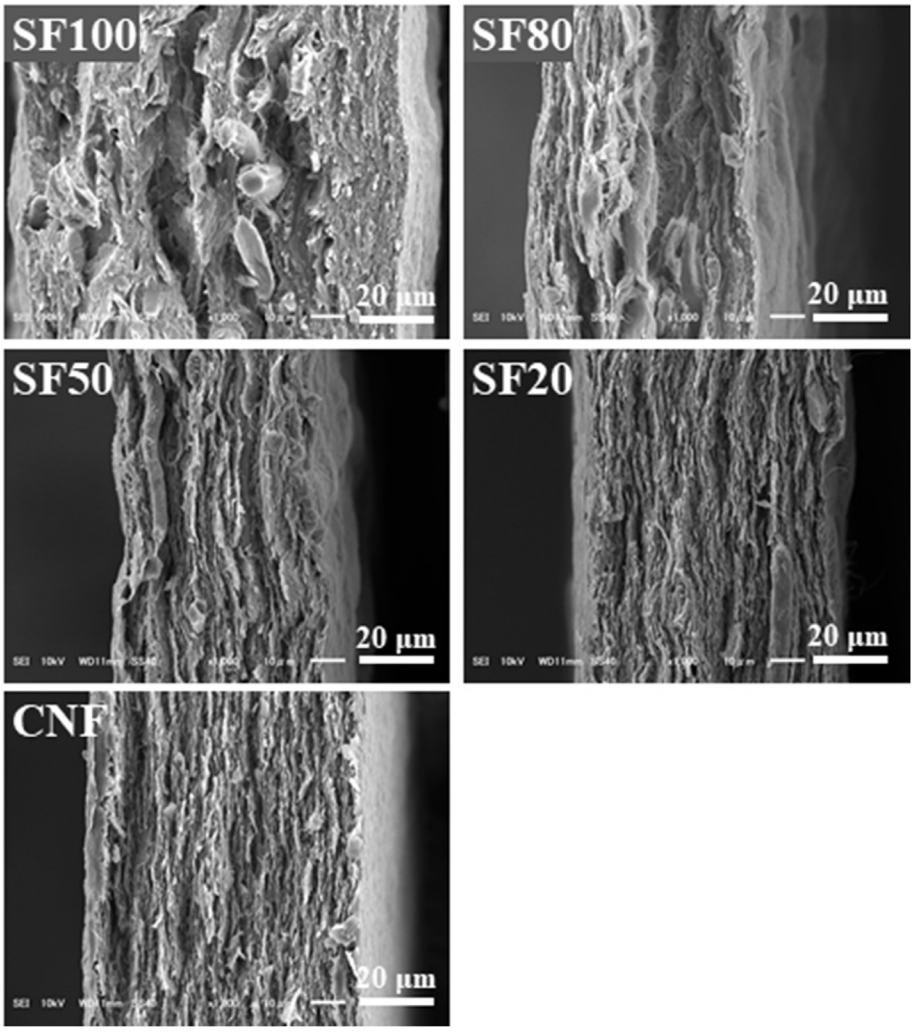

Fig. 10. SEM images of fracture surface after tensile test.

prepared using the new method in this study was improved by more than 13 °C, and the thermal decomposition peak of the composite films compounded with more than CNF 50 wt% showed almost the same temperature as the CNF film. Additionally, the mechanical properties of the composite films were increased with an increase in the amount of CNF. In particular, the strain at break of SF50 showed the longest value, as compared with the other composite films. These results suggest that a film using solutions directly fibrillated by a grinder leads to not only heat resistance, but also excellent mechanical properties as compared to films prepared by dissolving fibroin in a concentrated neutral salt. We strongly propose that our novel grinder treatment method makes it possible to readily overcome the poor solubility of silk fibroin in water. This environmentally friendly cellulose nanofiber/silk fibroin composite films will open many possibilities in biomaterials for tissue engineering, drug delivery systems, and biomedical applications. The development of continuous treatment processes is also in progress for an industrial scale.

Acknowledgements

This work was supported by a scholarship from the Kyoto Institute of Technology, and partially supported by the Center for Fiber & Textile Science, Kyoto Institute of Technology. The authors would like to acknowledge Daio Paper Corp., Japan, which supplied the cellulose nanofiber solution used in our research. The authors thank Mr. Kazuki Horii and Mr. Osamu Nagasuna at Nagasuna Mayu Inc. for kindly providing fibroin samples.

Appendix A. Supplementary data

Supplementary data to this article can be found online at https://doi.org/10.1016/j.jclepro.2019.06.215.

References

Bhardwaj, N., Kundu, S.C., 2011. Silk fibroin protein and chitosan polyelectrolyte complex porous scaffolds for tissue engineering applications. Carbohydr. Polym. 85 (2), 325–333.
Chen, L., Hu, J., Ran, J., Shen, X., Tong, H., 2014. Preparation and evaluation of collagen-silk fibroin/hydroxyapatite nanocomposites for bone tissue engineering. Int. J. Biol. Macromol. 65, 1–7.
Cho, S.Y., Lee, M.E., Choi, Y., Jin, H.-J., 2014. Cellulose nanofiber-reinforced silk fibroin composite film with high transparency. Fibers Polym. 15 (2), 215–219.
Du, C., Jin, J., Li, Y., Kong, X., Wei, K., Yao, J., 2009. Novel silk fibroin/hydroxyapatite composite films: structure and properties. Mater. Sci. Eng. C 29 (1), 62–68.
Farokhi, M., Mottaghitalab, F., Samani, S., Shokrgozar, M.A., Kundu, S.C., Reis, R.L., Fatahi, Y., Kaplan, D.L., 2018. Silk fibroin/hydroxyapatite composites for bone tissue engineering. Biotechnol. Adv. 36 (1), 68–91.
Feng, Y., Li, X., Li, M., Ye, D., Zhang, Q., You, R., Xu, W., 2017. Facile preparation of biocompatible silk fibroin/cellulose nanocomposite films with high mechanical performance. ACS Sustain. Chem. Eng. 5 (7), 6227–6236.

Gil, E.S., Frankowski, D.J., Bowman, M.K., Gozen, A.O., Hudson, S.M., Spontak, R.J., 2006. Mixed protein blends composed of gelatin and Bombyx mori silk Fibroin: effects of solvent-induced crystallization and composition. Biomacromolecules 7 (3), 728–735.
Gleick, P.H., 2003. Global freshwater resources: soft-path solutions for the 21st century. Science 302 (5650), 1524–1528.
Jin, J., Hassanzadeh, P., Perotto, G., Sun, W., Brenckle, M.A., Kaplan, D., Omenetto, F.G., Rolandi, M., 2013. A biomimetic composite from solution self-assembly of chitin nanofibers in a silk fibroin matrix. Adv. Mater. 25 (32), 4482–4487.
Kim, H.J., Yang, Y.J., Oh, H.J., Kimura, S., Wada, M., Kim, U.-J., 2017. Cellulose–silk fibroin hydrogels prepared in a lithium bromide aqueous solution. Cellulose 24 (11), 5079–5088.
Kundu, J., Mohapatra, R., Kundu, S.C., 2011. Silk fibroin/sodium carboxymethylcellulose blended films for biotechnological applications. J. Biomater. Sci. Polym. Ed. 22 (4–6), 519–539.
Lawrence, B.D., Wharram, S., Kluge, J.A., Leisk, G.G., Omenetto, F.G., Rosenblatt, M.I., Kaplan, D.L., 2010. Effect of hydration on silk film material properties. Macromol. Biosci. 10 (4), 393–403.
Lee, J.H., Bae, Y.S., Kim, S.J., Song, D.W., Park, Y.H., Bae, D.G., Choi, J.H., Um, I.C., 2018. Preparation of new natural silk non-woven fabrics by using adhesion characteristics of sericin and their characterization. Int. J. Biol. Macromol. 106, 39–47.
Liu, C.F., Xu, F., Sun, J.X., Ren, J.L., Curling, S., Sun, R.C., Fowler, P., Baird, M.S., 2006. Physicochemical characterization of cellulose from perennial ryegrass leaves (Lolium perenne). Carbohydr. Res. 341 (16), 2677–2687.
Lu, Q., Hu, X., Wang, X., Kluge, J.A., Lu, S., Cebe, P., Kaplan, D.L., 2010. Water-insoluble silk films with silk I structure. Acta Biomater. 6 (4), 1380–1387.
Marsano, E., Corsini, P., Canetti, M., Freddi, G., 2008. Regenerated cellulose-silk fibroin blends fibers. Int. J. Biol. Macromol. 43 (2), 106–114.
Mehrabani, M.G., Karimian, R., Mehramouz, B., Rahimi, M., Kafil, H.S., 2018. Preparation of biocompatible and biodegradable silk fibroin/chitin/silver nanoparticles 3D scaffolds as a bandage for antimicrobial wound dressing. Int. J. Biol. Macromol. 114, 961–971.
Ming, J., Liu, Z., Bie, S., Zhang, F., Zuo, B., 2014. Novel silk fibroin films prepared by formic acid/hydroxyapatite dissolution method. Mater Sci Eng C Mater Biol Appl 37, 48–53.
Monti, P., Freddi, G., Bertoluzza, A., Kasai, N., Tsukada, M., 1998. Raman spectroscopic studies of silk fibroin from Bombyx mori. J. Raman Spectrosc. 29 (4), 297–304.
Motta, A., Fambri, L., Migliaresi, C., 2002. Regenerated silk fibroin films: thermal and dynamic mechanical analysis. Macromol. Chem. Phys. 203 (10-11), 1658–1665.
Noishiki, Y., Nishiyama, Y., Wada, M., Kuga, S., Magoshi, J., 2002. Mechanical properties of silk fibroin–microcrystalline cellulose composite films. J. Appl. Polym. Sci. 86 (13), 3425–3429.
Okahisa, Y., Furukawa, Y., Ishimoto, K., Narita, C., Intharapichai, K., Ohara, H., 2018. Comparison of cellulose nanofiber properties produced from different parts of the oil palm tree. Carbohydr. Polym. 198, 313–319.
Okahisa, Y., Narita, C., Yamada, K., 2019. Preparation of silk-fibroin nanofiber film with native β-sheet structure via a never dried-simple grinding treatment. Journal of Fiber Science and Technology 75 (4), 29–34.
Singh, B.N., Panda, N.N., Mund, R., Pramanik, K., 2016. Carboxymethyl cellulose enables silk fibroin nanofibrous scaffold with enhanced biomimetic potential for bone tissue engineering application. Carbohydr. Polym. 151, 335–347.
Tsuboi, Y., Ikejiri, T., Shiga, S., Yamada, K., Itaya, A., 2001. Light can transform the secondary structure of silk protein. Appl Phys a-Mater 73 (5), 637–640.
Wang, R., Zhu, Y., Shi, Z., Jiang, W., Liu, X., Ni, Q.-Q., 2018. Degumming of raw silk via steam treatment. J. Clean. Prod. 203, 492–497.
Wiley, J.H., Atalla, R.H., 1987. Band assignments in the Raman spectra of celluloses. Carbohydr. Res. 160, 113–129.
Xie, X., Zhang, T., Gu, J., Huang, Z., 2018. Water footprint assessment of coal-based fuels in China: exploring the impact of coal-based fuels development on water resources. J. Clean. Prod. 196, 604–614.
Yamada, K., Tsuboi, Y., Itaya, A., 2003. AFM observation of silk fibroin on mica substrates: morphologies reflecting the secondary structures. Thin Solid Films 440 (1–2), 208–216.
Yang, G., Zhang, L., Liu, Y., 2000. Structure and microporous formation of cellulose/silk fibroin blend membranes: I. Effect of coagulants. J. Membr. Sci. 177 (1), 153–161.
Yano, H., Nakahara, S., 2004. Bio-composites produced from plant microfiber bundles with a nanometer unit web-like network. J. Mater. Sci. 39 (5), 1635–1638.
Yuan, Q., Yao, J., Huang, L., Chen, X., Shao, Z., 2010. Correlation between structural and dynamic mechanical transitions of regenerated silk fibroin. Polymer 51 (26), 6278–6283.
Zhang, H., Magoshi, J., Becker, M., Chen, J.Y., Matsunaga, R., 2002. Thermal properties ofBombyx mori silk fibers. J. Appl. Polym. Sci. 86 (8), 1817–1820.
Zhou, Z., Shi, Z., Cai, X., Zhang, S., Corder, S.G., Li, X., Zhang, Y., Zhang, G., Chen, L., Liu, M., Kaplan, D.L., Omenetto, F.G., Mao, Y., Tao, Z., Tao, T.H., 2017. The use of functionalized silk fibroin films as a platform for optical diffraction-based sensing applications. Adv. Mater. 29 (15).
Zhu, H., Liu, N., Feng, X., Chen, J., 2012. Fabrication and characterization of silk fibroin/bioactive glass composite films. Mater. Sci. Eng. C 32 (4), 822–829.